Computer Aided Diagnosis System for Lumbar Spine *

Raja' S. Alomari, PhD†
The University at Buffalo, SUNY
Buffalo, NY
ralomari@buffalo.edu

Vipin Chaudhary, PhD‡
The University at Buffalo, SUNY
Buffalo, NY
vipin@buffalo.edu

Gurmeet Dhillon, MD§
ProScan Imaging Inc.
Williamsville, NY
gdhillon@proscan.com

ABSTRACT

Lower back pain is the second most common neurological ailment in the United States after headache with over 12 million Americans having intervertebral disc disease (IDD). An emerging need for a Computer-Aided Diagnosis (CAD) system is due to the increasing number of patients (about 8%) that is not correlated with an increase in radiologists (about 1%). Thus, utilization of radiologists' time by having CAD systems is necessary to maintain the quality of the patient service. Furthermore, inter- and intra-radiologists variability in decision-making especially between novice and experienced teams urge the necessity of CAD systems that aid in presenting radiologists with reproducible diagnosis results. The design of a clinical CAD system requires active collaboration between computer scientists, engineers, and health professionals. In this paper, we present our efforts for designing a clinical CAD system for lumbar area. We closely work to integrate all our proposed machine-learning CAD methods within the clinical routine of our collaborating radiologist. We present the work flow of our system and its minimal interaction with the PACS system.

ISABEL '11, October 26-29, Barcelona, Spain

†Research Associate Fellow with the Dept of Computer Science and Engineering, SUNY at Buffalo.

‡Associate Professor with the Dept of Computer Science and Engineering, SUNY at Buffalo.

§Radiologist and owner of ProScan Inc. at Buffalo, Williamsville, NY

Categories and Subject Descriptors

J.3 [**Computer Applications**]: LIFE AND MEDICAL SCIENCES

Keywords

Computer-aided diagnosis; Lumbar MRI; PACS; Clinical work flow; MRI

1. INTRODUCTION

Computer-Aided Diagnosis (CAD) research has been gaining substantial attention from the medical imaging community. There is a large corpus CAD research papers for many organs in the body using various possible medical imaging modalities. A few CAD systems have been utilized within the clinical work flow as both experimental setting and commercial products. Major focus of these CAD systems are on life threatening diseases such as cancers [12, 13, 14] and well-funded projects such as nodule-detection from lungs CT images [16].

CAD has become an integral part of the clinical routine for screening and detection of several types of abnormalities in medical imaging. Moreover, the increasing demand on diagnosis from radiology scans has been attracting many researchers to integrate CAD into radiologists work flow to efficiently utilize radiologists' time and provide computerized algorithms for diagnosis and clinical report generation [9]. However, the lack of integration of CAD with the PACS (Picture archiving and communication system) has been one of the biggest barriers for utilizing the many CAD research efforts [10]. Furthermore, the lack of a clinical standard for specific abnormality across various clinics and hospitals add to the burden of generalizing CAD systems and integrating them within the clinical work flow.

Fig. 2 shows the typical work flow of the clinical setting. Initially, the technician administers MRI acquisition for all sagittal, axial, and rotational views. The full MRI is then saved in a central database along with patient information record. Then using the DICOM viewer, the radiologist visualizes the images and diagnoses the case which is stored back in the central database. The diagnosis interface automatically generates the diagnosis report based on the manual radiologist input in a standard form.

Our main research focus is on CAD for lumbar area that we call our collective system: LumbarCAD. There has been various research efforts that target the lumbar spine area including ours [1, 2, 6, 5, 3]. However, the integration of these efforts within the clinical work flow requires special attention and is

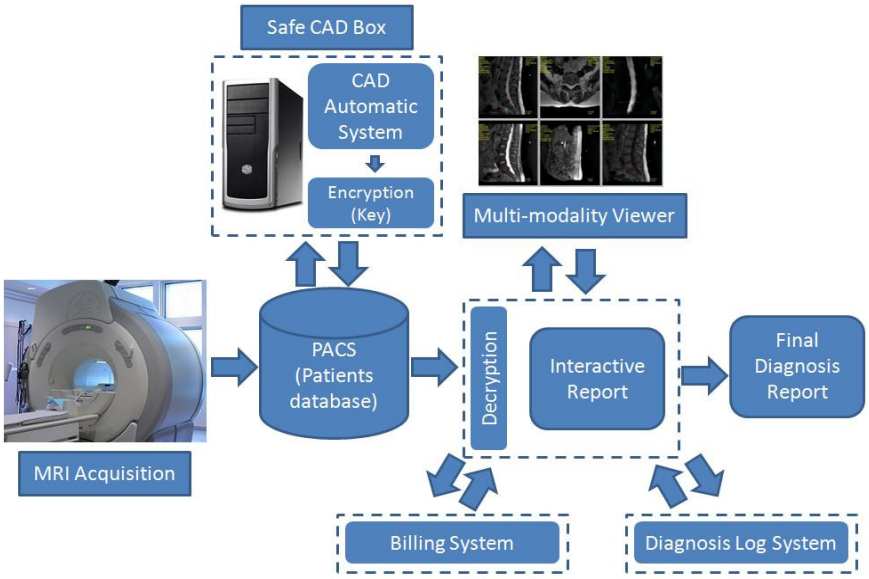

Figure 1: Clinical work flow of lumbar diagnosis. LumbarCAD main components in dashed boxes.

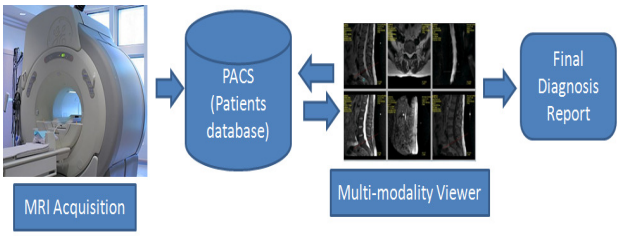

Figure 2: Clinical work flow of lumbar diagnosis.

highly dependent on the clinical setting that greatly varies from one clinic to another. The variations include the PACS system access, imaging modalities, and even the acquisition protocols and resulting images. In this paper, we present our LumbarCAD system that we integrate within the work flow of our collaborating radiology center. We describe the clinical setting and the data acquisition protocols and how our LumbarCAD system integrates seamlessly.

2. PROPOSED LUMBAR CAD SYSTEM

The integration of our collective CAD system within the work flow of the clinical routine faces many challenges starting from the variability in platforms, the access to PACS, the access to the viewer, and, more importantly, the convenience of the radiologist so that we don not change the clinical workflow. Our LumbarCAD system has four standalone components to the clinical routine highlighted by the dashed boxes in Fig. 1.

2.1 Safe CAD Box: Automatic CAD System

This module represents a black-box processing unit, that we provide. It interacts with the PACS via SQL query protocol to acquire full MRI case (or a batch of cases) and save back the case (after inserting our diagnosis within the DICOM header) to the PACS. This processing unit contains the research part of the automated labeling and diagnosis of lumbar spine. We save the resulting labeling and diagnosis information in a data structure; then we encrypt the data structure and store the resulting information in specific attributes within the header file of specific protocols within the MRI case. We duplicate storage of this information in multiple headers for fault tolerance purposes. This "Safe CAD Box" stays on site to eliminate the risk of any patient information leak and preserve their privacy. The encryption key is unique for each of these processing boxes. In the current status of our system, we integrated our labeling [1], herniation [5, 6, 8], and desiccation [3] diagnosis.

2.2 Interactive Diagnosis Report

This module provides an interactive automated diagnosis report. It allows the radiologist to fetch patient information and presents the radiologist with an interactive report showing automated diagnosis results with confidence for each decision. It allows the radiologist to invoke the DICOM viewer to manually verify the results and edit the diagnosis manually. This interface contains the decryption key to decrypt the automated diagnosis information.

2.3 Diagnosis Log System

This system keeps track of the cases along with the automated and manual decisions. This is useful for building the training data for future enhancements of our automatic CAD system. This module prepares the necessary data to re-train the automatic supervised machine learning algorithms. Ground truth becomes the manual decision of the radiologist for every case. Ultimately, it will enhance the automatic decision and adapt it to the radiologist decisions.

2.4 Billing System

This system keeps track of the usage of the automated decision. We have two billing models: pay-per-use and license-based. Pay-per-use enters a log for the billing system whenever the decryption step is performed and it is triggered every time the radiologist wants to see the automated results. On the other hand, the license-based billing model allows a certain time frame of usage.

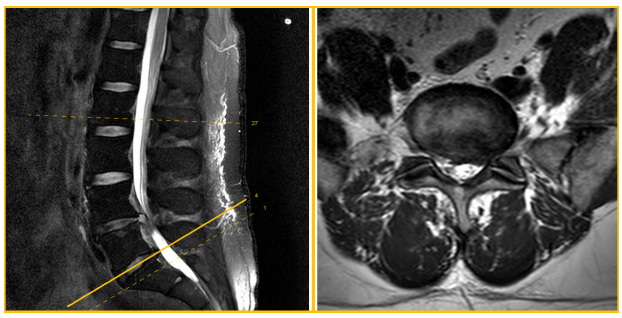

Figure 3: Sample slice from the six axial slices for the L5-S1 disc.

3. CLINICAL DATA

Clinical MRI data for lumbar spine diagnosis varies across various clinics and hospitals. However, there are some common acquisition protocols. Specifically, for our LumbarCAD system, we customize it to fit the available clinical MRI. Initially, the technician acquires a survey view which is a lower quality quick scan of the lower spine including sagittal and coronal views. This step helps the technician determine the positioning of the patient and decide the acquisition protocols.

Then the technician acquires sagittal views consisting of twelve to fourteen slices for both T1- and T2-weighted protocols. Then she manually plans for the axial views where she draws a bounding box around each of the discs starting from the L5-S1 up to L1-L2 or T12-L1 depending on the initial judgment of the case and whether abnormalities might be noticed on the higher discs. The acquisition protocols produces six axial slides per disc in the orientation specified by the technician. This guarantees that the axial slices are parallel, to the best that a technician can have, with the major axis of the disc. Axial views are T1-weighted MRI. Finally, the technician acquires a lateral rotational back view for the lumbar spine using Myelo protocol. This Myelo protocol shows only the thecal sac suppressing all other structures in that area. During this whole time, the patient is asked not to move at all and if any movement in the position happens, the entire process is repeated. This guarantees the registration of all views on each other. It takes approximately 24 minutes for the whole acquisition for one case. Fig. 3 shows an example of an axial slice from the six axial slices for the L5-S1 disc.

Our dataset that we have been using exceeds one thousand cases that has been acquired over the last six years (2006 - 2011) on both 1.5 and 3 Tesla Philips Intera MRI scanners. Over 90% of the cases are cases on the 3 Tesla machine. Patient ages varies between 17 to 83 years old.

4. TECHNICAL VIEW

Within the automatic CAD system, there are two main steps to automate: labeling and diagnosis. Labeling includes detection of discs and naming them based on the anatomical convention. Then diagnosis tasks are executed serially to obtain the automated diagnosis result for each abnormality. Our area of interest includes the discs from L5-S1 up to T12-L1.

4.1 Localization and Labeling

We refer to the labeling problem as naming each disc level upon the anatomical naming convention for discs from L5-S1 up to T12-L1. On the other hand, localization refers to having a point within the boundary of each disc. This point is useful for producing a bounding box around each disc in preparation for the CAD methods for diagnosis.

We perform labeling of the discs on the sagittal view utilizing our two-level probabilistic model proposed in [1]. We marginalize over the possible disc-labellings $\mathcal{D}$ since these are auxiliary variables giving the following optimization function:

$$\begin{aligned}\mathcal{D}^* &= \arg\max_{\mathcal{D}} \sum_{\mathcal{L}} P(\mathcal{L}, \mathcal{D}|\mathtt{I}) \\ &= \arg\max_{\mathcal{D}} \sum_{\mathcal{L}} \frac{P(\mathtt{I}|\mathcal{D}, \mathcal{L})P(\mathcal{D}, \mathcal{L})}{P(\mathtt{I})} \\ &= \arg\max_{\mathcal{D}} \sum_{\mathcal{L}} P(\mathtt{I}|\mathcal{L})P(\mathcal{L}|\mathcal{D})P(\mathcal{D}) \qquad (1)\end{aligned}$$

where the second equality follows from the multi-level nature of the model (the disc variables are assumed independent of the intensities) and the $P(\mathtt{I})$ in the denominator is independent of the maximization over $\mathcal{D}$ and can be ignored. Note the summation is over a very large set of possible assignments ($2^{|\Lambda|}$). We model it as a Gibbs distribution:

$$P(\mathtt{I}|\mathcal{L}) = \frac{1}{Z[\mathtt{I}|\mathcal{L}]} \exp\Big[-\beta_1 \sum_{s\in\Lambda} U_{\mathrm{I}}(l_s, \mathtt{I}(s))\Big] \quad \leftarrow \text{intensity} \qquad (2)$$

$$P(\mathcal{L}|\mathcal{D}) = \frac{1}{Z[\mathcal{L}|\mathcal{D}]} \exp\Big[-\beta_2 \sum_{s\in\Lambda} U_{\mathrm{D}}(l_s, \mathcal{D})\Big] \quad \leftarrow \text{spatial} \qquad (3)$$

$$P(\mathcal{D}) = \frac{1}{Z[\mathcal{D}]} \exp\Big[-\beta_3 \sum_{d_i\in\mathcal{D}} U_{\mathrm{L}}(d_i) \quad \leftarrow \text{location} \\ -\beta_4 \sum_{(i\sim j)} V_{\mathrm{D}}(d_i, d_j)\Big] \quad \leftarrow \text{context} \qquad (4)$$

where s is a pixel on the lattice Λ ($s \in \Lambda$), $\mathtt{I}(s)$ is the intensity level of the pixel s, $\beta_k \geq 0, k = \{1, \ldots, 4\}$ are tunable parameters, the $(\cdot \sim \cdot)$ notation denotes the set of neighboring elements on the disc chain. $Z[\mathtt{I}|\mathcal{L}]$, $Z[\mathcal{L}|\mathcal{D}]$, and $Z[\mathcal{D}]$ are the partition functions that make the normalizing constant for the Gibbs distribution for each model, respectively. The potentials $U_{\mathrm{I}}(l_s, \mathtt{I}(s))$ and $U_{\mathrm{D}}(l_s, \mathcal{D})$ describe the low-level disc intensity and the spatial relationship at the disc level, respectively, while the potentials $U_{\mathrm{L}}(d_i)$ and $V_{\mathrm{D}}(d_i, d_j)$ describe the high-level object location and context, respectively. Both i and j are indexes for the six discs centers xy-coordinates. All four potentials are discussed in detail in the next two subsections.

The first level, $P(\mathtt{I}|\mathcal{L})P(\mathcal{L}|\mathcal{D})$, captures the probability of a particular labeling given both the underlying image and the overlying disc variables. Each potential function models a different aspect of the local pixel-level information (the aspect is mentioned on the right of each equation-line). The second level $P(\mathcal{D})$ models the high-level information about the disc locations and context.

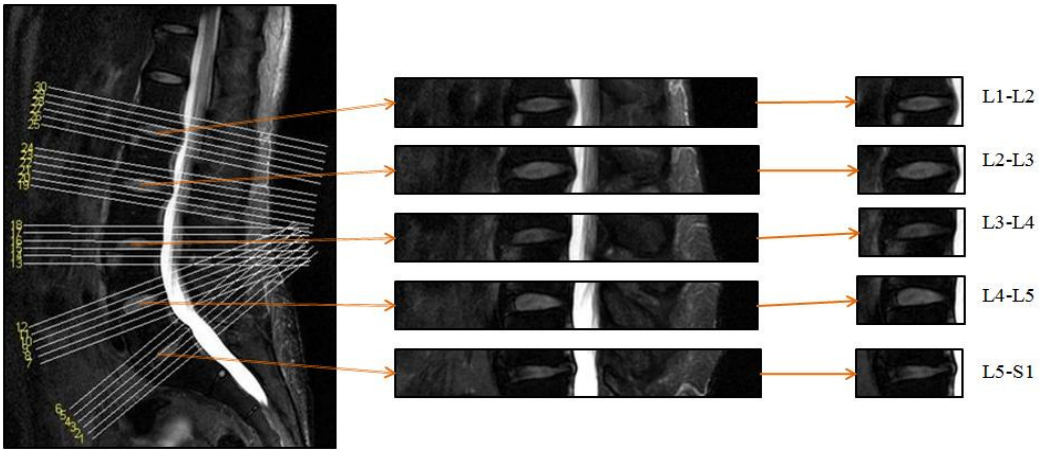

Figure 4: This figure shows the extraction of a rough bounding box for each disc in the sagittal mid-slice using information from the corresponding axial slices and subsequently giving a tighter bounding box in the anterior-posterior direction.

To prepare for the diagnosis step, we produce a bounding box surrounding each disc. To obtain such bounding boxes we utilize the axial views geometry as follows:

- Extraction of rough bounding box: In this step we use the lower and upper intersecting line of the mid-sagittal.
- Tightening the bounding box: the previous step delimits the disc from top-bottom , but not in the anterior-posterior direction. We detect the high-intensity spinal cord on the right-hand side of each disc in $R1$ and hence get a right side cut-off. For the left side, we empirically set $2/9^{th}$ of the width of $R1$ to get the cut-off, finally resulting in a better bounding box for each disc as illustrated in Fig. 4.

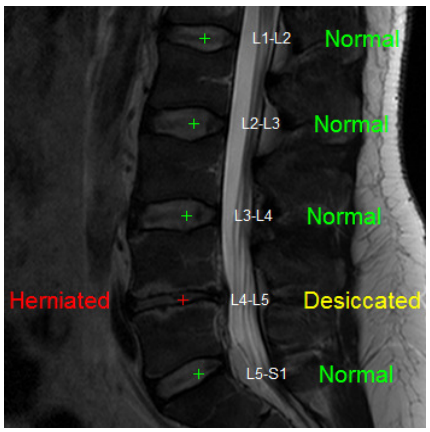

Figure 5: LumbarCAD results projected on a Mid-Sagittal clinical MRI.

4.2 Automated Diagnosis

We have been developing the CAD system for diagnosis of various lumbar spine abnormalities from MRI [7, 15, 11]. Until now we have incorporated two major abnormalities in the lumbar discs, namely: disc herniation [7, 11] and desiccation [3]. We proposed many other CAD efforts but they are still under thorough testing to meet the clinical accuracy before being incorporated in LumbarCAD system.

For herniation diagnosis, we presented a fully automated herniation detection system [8] using GVF snake for an initial disc contour and a Bayesian classifier. Initially, we apply a range filter on the images to produce an edge map from the sagittal views [7]. Both the point inside the disc and the edge map (initial contour) are used to initiate the GVF-snake from within the disc. This guarantees that the final disc segmentation lies within the disc and thus a successful segmentation. Once the segmentation is performed, we use a build a binary Bayesian classifier:

$$n^* = \arg\max_n P(n|\mathtt{S}) \tag{5}$$

where n is a binary random variable stating whether it is a herniated or a normal disc, $\mathtt{S}$ incorporates shape features extracted from GVF-snake final contour. We utilize a Gibbs distribution with two shape potentials:

$$P(n|\mathtt{S}) = \frac{1}{Z[n]} \exp^{-[\alpha_1 U_{\mathrm{S1}} + \alpha_2 U_{\mathrm{S2}}]} \tag{6}$$

where $\mathtt{S}$ represents the shape features extracted from the GVF-snake, $Z[n]$ is the normalization factor of the Gibbs distribution, α_1 and α_2 are tuning parameters. We define two shape potentials: 1) U_{S1} models the major axis of the GVF-snake final contour . 2) U_{S2} models the minor axis of the GVF-snake final contour. Detailed are outlined in [8]

For Desiccation, we utilize our algorithm that uses a probabilistic model that incorporates intervertebral disc appearance and contextual information for automating the diagnosis of lumbar disc desiccation [4]. We capture desiccation (loss of disc water contents) n_i with a Gibbs model:

$$P(n_i|d_i, \sigma_{\mathtt{I}(d_i)}) = \frac{1}{Z[n_i]} \exp^{-\mathcal{E}_{n_i}(d_i, \sigma_{\mathtt{I}(d_i)})} \quad (7)$$

where n_i is a binary random variable for desiccation of the disc i and $n_i \in \mathcal{N} = \{n_i : 1 \leq i \leq 6\}$; d_i is the location of the disc i and $d_i \in \mathcal{D} = \{d_i : 1 \leq i \leq 6\}$; σ_{d_i} is a neighborhood of pixels around the disc location d_i. $\mathcal{E}_{n_i}(d_i, \sigma_{\mathtt{I}(d_i)})$ is the energy function identified by disc location d_i and the intensity of a pixel neighborhood $\sigma_{\mathtt{I}(d_i)}$.

We use two potentials that represent the appearance $\mathtt{I}$ and the context in intensity between discs ($i \sim j$). Our energy function is:

$$\mathcal{E}_{n_i}(d_i, \sigma_{\mathtt{I}(d_i)}) = \Big[\beta_1 \sum_{d \in \mathcal{D}} U_{\mathrm{I}}(d_i, \sigma_{\mathtt{I}(d_i)}) + \beta_2 \sum_{(i \sim j)} V_{\mathrm{D}}(\widetilde{\sigma_{\mathtt{I}(d_i)}}, \widetilde{\sigma_{\mathtt{I}(d_j)}}; n_i, n_j)\Big] \quad (8)$$

where β_1 and β_2 are the model parameters that control the effect of appearance and context on the inference. $\widetilde{\sigma_{\mathtt{I}(d_i)}}$ is the median intensity level for the disc pixel neighborhood $\sigma_{\mathtt{I}(d_i)}$. U_{I} is the appearance potential which is a model of disc intensity neighborhood surrounding each disc $d_i \in \mathcal{D}$ and the intensity of the pixel neighborhood $\sigma_{\mathtt{I}(d_i)}$ of that location. V_{D} is the context potential which we model as a Bayesian model-aware affinity that handles context $\mathcal{D}$ between neighboring discs ($i \sim j$). The general framework for our methods utilizes various intra- and inter-discs features. We also approach the diagnosis tasks via typical machine learning methods includingNeural Networks, SVM, and others [11].

5. CONCLUSION

We presented an overview of our LumbarCAD system and our efforts in integration of the CAD system within PACS. Our LumbarCAD system consists of four standalone modules that have limited interaction with PACS only with minimal interaction. The four components are: The Safe CAD Box, interactive diagnosis report, diagnosis log system, and the billing system. The Safe CAD Box implements the combination of our published research efforts in lumbar discs labeling, detection, and diagnosis. We presented a technical overview of the methods for both herniation and desiccation. The interactive diagnosis report system comprises an interface for the radiologist that interacts with the PACS through SQL query, presents the radiologist with the automated diagnosis report, allows him to manually change any result by invoking the DICOM viewer, and then print out the final report. The third component keeps track of each case along with the automatic and manual diagnosis. This will incrementally collect training data for our CAD algorithms for future enhancements. The last component is for billing purposes where we provide either a pay-per-view model or a license-based billing model. Our LumbarCAD is now fully functional within a testing environment.

6. ACKNOWLEDGMENT

Authors would like to acknowledge the efforts of both the PhD students: Jaehan Koh and Subarna Ghosh for helping get this work done.

7. REFERENCES

[1] R. Alomari, J. Corso, and V. Chaudhary. Labeling of lumbar discs using both pixel- and object-level features with a two-level probabilistic model. *IEEE Trans. in Medical Imaging*, 30:1–10, 2011.

[2] R. Alomari, J. Corso, V. Chaudhary, and G. Dhillon. Abnormality detection in lumbar discs from clinical MR images with a probabilistic model. *CARS'09*, 2009.

[3] R. Alomari, J. Corso, V. Chaudhary, and G. Dhillon. Desiccation diagnosis in lumbar discs from clinical MRI with a probabilistic model. *ISBI'09*, page 546Ű549, 2009.

[4] R. Alomari, J. Corso, V. Chaudhary, and G. Dhillon. Desiccation diagnosis in lumbar discs from clinical mri with a probabilistic model. pages 546–549, 2009.

[5] R. Alomari, J. Corso, V. Chaudhary, and G. Dhillon. Automatic diagnosis of disc herniation with shape and appearance features from MRI. *Proc. SPIE'10 Medical imaging*, 2010.

[6] R. S. Alomari, J. Corso, V. Chaudhary, and G. Dhillon. Computer-aided diagnosis of lumbar disc pathology from clinical lower spine MRI. *IJCARS*, 5(3):287–293, 2010.

[7] R. S. Alomari, J. Corso, V. Chaudhary, and G. Dhillon. Computer-aided diagnosis of lumbar disc pathology from lower spine MRI. *IJCARS'10*, 5(3):287–293, 2010.

[8] R. S. Alomari, J. Corso, V. Chaudhary, and G. Dhillon. Toward a clinical lumbar cad: Herniation diagnosis. *International Journal of Computer Aided Radiology and Surgery*, 6(1):119–26, 2011.

[9] K. Doi. Computer-aided diagnosis in medical imaging: Historical review, current status and future potential. *Computerized Medical Imaging and Graphics*, 31:198–211, 2007.

[10] D. Domino. Integration of cad with pacs breaks down barrier to its use. *Diagnostic Imaging*, 31(7), 2009.

[11] S. Ghosh, R. Alomari, V. Chaudhary, and G. Dhillon. Computer-aided diagnosis for lumbar MRI using heterogeneous classifiers. pages 1179–1182, 2011.

[12] iCAD. Second look digital from iCAD. *Computer Aided Diagnosis Tool*, 2009.

[13] iCAD. Spectra look digital from iCAD. *Computer Aided Diagnosis Tool*, 2009.

[14] iCAD. Vivid look from iCAD. *Computer Aided Diagnosis Tool*, 2009.

[15] J. Koh, R. Alomari, V. Chaudhary, and G. Dhillon. Lumbar spinal stenosis CAD from clinical MRM and MRI based on inter- and intra-context features with a two-level classifier. volume 7963, 2011.

[16] C. White, R. Pugatch, T. Koonce, S. Rust, and E. Dharaiya. Lung nodule cad software as a second reader: A multicenter study. *Academic Radiology*, 15(3):326–333, 2008.